IEEE Access
Multidisciplinary | Rapid Review | Open Access Journal

Received July 13, 2021, accepted July 17, 2021, date of publication July 20, 2021, date of current version July 30, 2021.

*Digital Object Identifier 10.1109/ACCESS.2021.3098846*

# Seawater Battery-Based Wireless Marine Buoy System With Battery Degradation Prediction and Multiple Power Optimization Capabilities

**JEONGHOON CHO[1], MYEONG WOO KIM[1], YOUNGJIN KIM[2], JEONG-SUN PARK[3], DO-HEE LEE[4], YOUNGSIK KIM[2], AND JAE JOON KIM[1], (Senior Member, IEEE)**

[1]Department of Electrical Engineering, Ulsan National Institute of Science and Technology (UNIST), Ulsan 44919, South Korea
[2]School of Energy and Chemical Engineering, Ulsan National Institute of Science and Technology (UNIST), Ulsan 44919, South Korea
[3]4TOONE Corporation, Ulsan 44919, South Korea
[4]IoT Convergence Technology Solution Company (STL), Ulsan 44421, South Korea

Corresponding authors: Youngsik Kim (ykim@unist.ac.kr) and Jae Joon Kim (jaejoon@unist.ac.kr)

This work was supported in part by the National Research Foundation of Korea (NRF) Grant funded by the Ministry of Science and ICT (MSIT) under Grant 2017M1A2A2087833, in part by the Basic Science Research Program through the NRF funded by the Ministry of Education under Grant 2020R1A6A1A03040570, and in part by the 2021 Research Fund of Ulsan National Institute of Science and Technology (UNIST) under Grant 1.200070.01.

**ABSTRACT** This paper presents a wireless marine buoy system based on the seawater battery (SWB), providing self-powered operation, power-efficient management, and degradation prediction and fault detection. Since conventional open circuit voltage (OCV) methods cannot be applied due to inherent cell characteristics of SWB, the coulomb counting (CC) method is adopted for the state of charge (SOC) monitoring. For the state of health (SOH), a variance-based detection scheme is proposed to provide degradation prediction and fault detection of the SWB. The self-powered operation is augmented by two proposed power optimization schemes such as multiple power management and three-step LED light control. A wireless buoy system prototype is manufactured, and its functional feasibility is experimentally verified, where its location and SOC are periodically monitored in a smartphone-based wireless platform.

**INDEX TERMS** Buoy system, seawater battery, coulomb counting, self-powered, degradation prediction, fault detection, multiple power optimization, state of charge, variance-based detection.

## I. INTRODUCTION

Recent demand for eco-friendly energy sources has been rapidly increasing [1]–[3] while the Lithium-ion battery (LIB) has been widely used thanks to high energy density and long-life span [4]–[6]. However, if the LIB is exposed to seawater or corroded by immersion, its cobalt toxicity causes serious environmental pollution problems [7]. Therefore, the seawater battery (SWB) is attracted as one of alternative to minimize the pollution problems, especially in marine environment applications [8]–[11]. Since it is composed of the sodium, which is abundant in ocean environments, the SWB can be a promising candidate to replace the high-cost LIB [8]. Also, via two main reactions of the oxygen evolution reaction (OER) upon charging and the oxygen reduction reaction (ORR) upon discharging, the SWB would be eco-friendly, which does not generate toxic materials [9]. Since the SWB operates with its cells submerged in the sea, it avoids the danger of being explode, and also has less affected by the temperature which is one of significant variables for battery management system (BMS) [10]. Besides, it has stable capacity that the coulombic efficiency is 98% during 600 cycles and more than 80% of energy efficiency [11].

Accordingly, there have been some attempts to apply the SWB to marine applications [12]–[15]. Marine application devices based on the SWB cells include the power plants [12], [13], the energy storage system (ESS) for boats [14], and the buoy for coastal positioning which is self-powered with other harvesting devices like the photovoltaic (PV) [15]. Especially, the buoy application is interested in its usage time [16], but there are still some issues to

The associate editor coordinating the review of this manuscript and approving it for publication was Shiwei Xia.

be resolved in these previous works. Firstly, it requires proper methods to support the state of charge (SOC) estimation function [17]–[21]. The SWB cell voltage during operations changes in proportion to the amount of charge or discharge since Na+ ions of seawater move to the inside of the anode to form Na metal during the charging process [17]. However, even if the amount of charge increases, only the amount of Na metal increases and the state of the material does not change [18]. Since it is driven in infinite seawater, the cell voltage is not affected [19]. Consequently, the SWB cells shows that the open circuit voltage (OCV) finally regress to constant cell voltage after its charge or discharge operations are done [20]. Because of these inherent SWB cell characteristics, conventional OCV-based SOC estimation methods would be not available [21]. Secondly, protection techniques are necessary to maintain stable battery state by preventing overcharge and undercharge as in the LIB [2], [22]. For the SWB operation through ORR or OER reactions, it is necessary to suppress unnecessary reactions by using a kind of cutoff voltage [23], [17].

Thirdly, for lifetime or optimal replacement time estimations, the degradation progress in the SWB cell needs to be informed. The carbon-based current collector is decomposed into gases such as $CO_2$ during the electrochemical reaction process. Also, discharge by-products may block the surface, reducing the reaction area which results in the degradation of the SWB [24]. In the case of LIB, there are several methods for measuring the degradation of the battery [25]–[31]. For the state of health (SOH) in the LIB, the present capacity based on the total discharge amount of the first cycle is compared, using the coulomb counting (CC)-based method [25] or model parameters as the relationship between SOH and OCV through laboratory tests [26], [27]. The Kalman filter method which can consider the various parameters of battery is proposed in [28]. As a data-driven approach such as the fuzzy logic, complex and nonlinear SOH is identified through a fuzzy rule set [29]. The artificial neural network (ANN) can process large amounts of data and variables accurately for the SOH estimation [30]. Additional other real data-based inconsistency evaluation methods [31] are also introduced previously for the LIB. However, many OCV-based SOH estimation methods cannot be applied due to the constant OCV regression characteristic of the SWB. In addition, the SWB is relatively recently developed compared to LIB, those data-based SOH estimation works for the SWB are rarely reported. Lastly, under marine environments, the buoy needs to be self-powered with harvesting devices such as PV [32], wind [33] and wave harvester [34] for long-lasting system operation. Also, intelligent power management techniques are required, since the buoy lightening causes large power consumption. Energy-efficient operation methods of LED lighting have been proposed in [35]–[37]. They include distributed lighting control with light sensing [35], regulating between artificial light and daylight. Additionally, the system meets the desired amount of light with minimal energy consumption in [36], and the optimal lighting decision algorithm and lighting control algorithm are proposed in [37] in order to satisfy both user needs as well as energy saving. However, these researches have been implemented mostly for indoor applications where they requires a bundle of cables to control the system, requiring more costs for installation and maintenance.

This paper proposes an eco-friendly wireless marine buoy system based on the SWB, implementing its performance degradation prediction and multiple power optimization. A proposed hybrid approach of OCV and CC, called variance-based detection scheme, prevents the SWB from functional hazards, providing capabilities of SOC and SOH. Two proposed power schemes of multiple power management and SWB save mode maximizes the system operating time for the self-powered operation. The buoy system information on battery status and geometric position are wirelessly transmitted to a long-term evolution (LTE) server. Its mobile service platform is designed to display periodically monitored real-time information of the intelligent marine buoys, allowing comfortable maintenance.

This paper is organized as follows. The proposed intelligent SWB-based buoy architecture is presented in Section II, and its system implementations are detailed in Section III. The experimental results are shown in Section IV, and the conclusion is drawn in Section V.

## II. SWB-BASED BUOY SYSTEM ARCHITECTURE

Fig. 1 shows the proposed intelligent SWB-based wireless buoy system. In Fig. 1(a), the proposed system diagram is composed of multiple power sources, a microcontroller unit (MCU), a power delivery circuit, LED array, and wireless communication circuits. For multiple power sourcing, the PV provides a self-powered energy source, and the SWB works as primary energy storage. A power delivery circuit together with the MCU predicts CC-based SWB performance degradation, which also provides SWB fault detection. For further power optimization capability, the three-step LED light control and the UPS function are included. Its wireless communication periodically delivers its geometrical buoy location and CCSOC information of the SWB to a system server. Fig. 1(b) shows a conceptual diagram of the proposed buoy system, where it takes the form of a cylindrical structure, both the PV and the LEDs are located at its top side. The upper central part has the main circuit module that provides the CC-based SWB degradation prediction and fault detection, the multiple power-source optimization, and the wireless communication. The SWB is placed at the bottom of the buoy. Fig. 1(c) shows its manufactured system prototype, the PV on its top part is coated with dome-shaped transparent seal to achieve maximum condensing function for the same insolation. The main circuit module and the UPS in the upper central part are protected from the sea water while the SWB in the bottom part is designed to be submerged into the sea water.

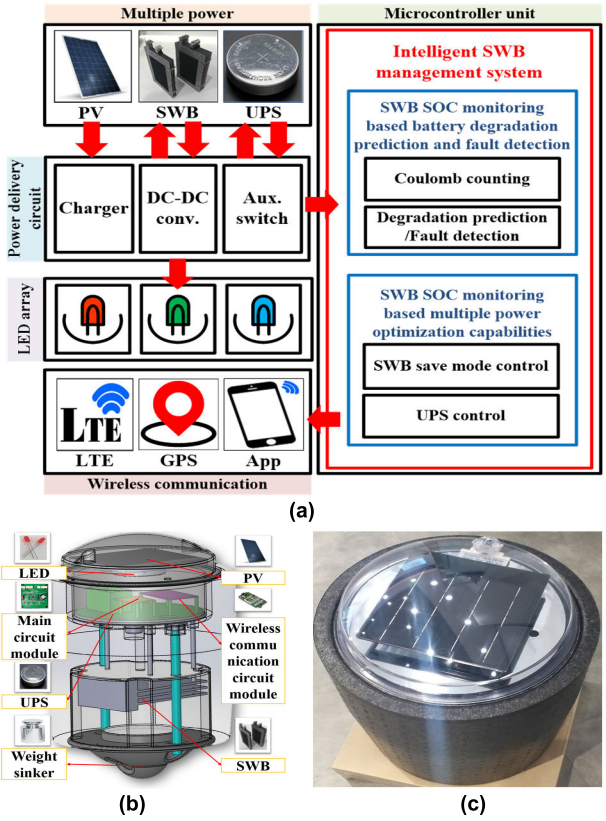


**FIGURE 1.** Proposed SWB-based wireless buoy system: (a) system diagram, (b) conceptual diagram, and (c) prototype photograph.

Fig. 2 shows a functional block diagram of the proposed buoy system, which is controlled by multiple power-source management circuit. Its power delivery operations are mainly divided into two paths. The red-colored (Path 1) charges the SWB with the PV, and turns on the LED by discharging the SWB. The blue-colored (Path 2) is composed of a charging path from the PV to the UPS, and a discharging path from the UPS to the LED. In addition, there is another path through an auxiliary switch to receive the discharged energy selectively from the SWB or the UPS. The MCU has five data of $V_{PV}$, $V_{UPS}$, $V_{SWB}$, $Q_{charge+}$, and $Q_{charge-}$ to manage the overall buoy system. Fig. 3 shows the operational flow chart of the proposed buoy system. After going through initial power-up sequence, the following operations are classified into two major processing algorithms of the SWB degradation prediction and the CCSOC-based multiple power optimizations. Firstly, the buoy system starts the coulomb counting operation, and it extracts the CCSOC of the SWB, periodically monitoring its battery voltage. Charging or discharging data from a CC sensing circuit are accumulated, and also its instant battery voltage is measured with an internal analog-to-digital converter (ADC) in the MCU. The variance of the battery voltage swing under charge/discharge time and amount conditions tends to become bigger as the SWB's performance aging proceeds. Based on the variance of the battery voltage swing range under iterative charge/discharge operations, the performance degradation amount or aging stages

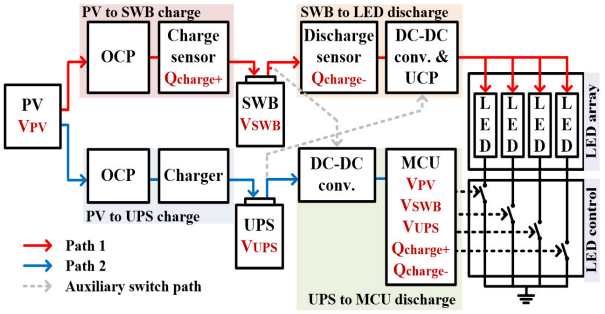


**FIGURE 2.** Functional block diagram of proposed buoy system.

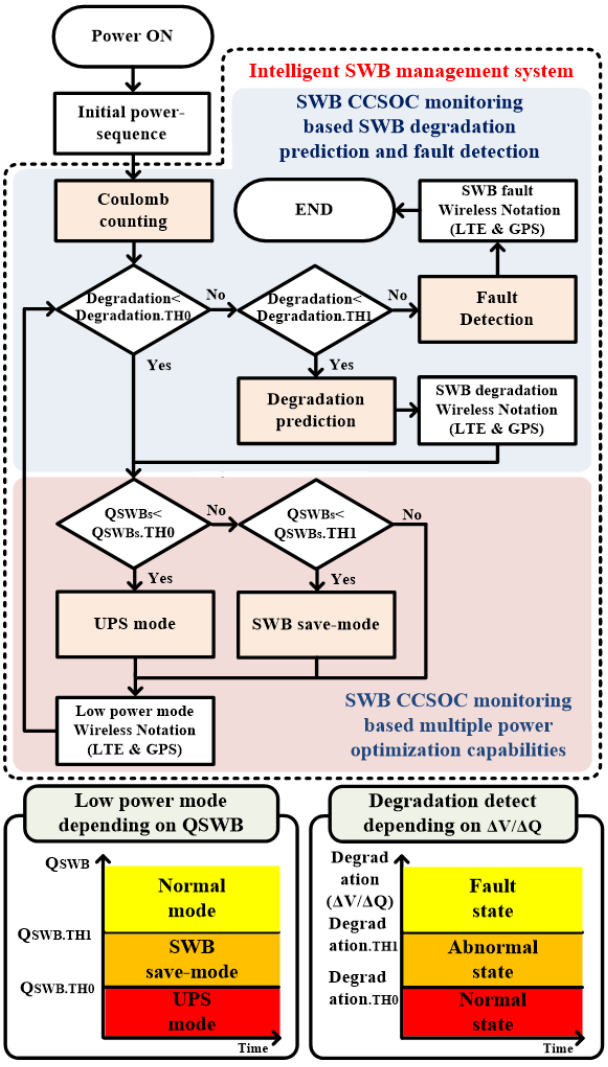


**FIGURE 3.** Operational flow chart of proposed buoy system.

of the SWB are estimated. If the estimated degradation is bigger than a first critical value of $\text{Degradation}_{\text{TH0}}$, the SWB is considered as under abnormal state. If it is further bigger than a second critical value of $\text{Degradation}_{\text{TH1}}$, the SWB is regarded as under fault state. Real-time information on the SWB's CCSOC is utilized for the battery safety protection. The overcharge protection function is performed before the

CCSOC exceeds a charging capacity limit. The undercharge protection is performed before the CCSOC falls below a discharging limit which might cause damage in the SWB.

Additionally, this buoy system is designed to perform multiple power optimizations for its sustainable or self-powered operation capability. It operates in the SWB save mode when the CCSOC of the SWB falls below a certain level ($Q_{SWB.TH1}$). The SWB save mode aims to reduce power consumption by controlling the lighting LED which contributes to major power-consuming factor in the overall buoy system. It maximizes the usage time from the residual SWB energy by using three control methods of LED number control, pulse-width modulation (PWM) control, and pulse-frequency modulation (PFM) control. When the CCSOC of the SWB is close to zero ($Q_{SWB.TH0}$), the buoy system is designed to proceed into the UPS mode for further extended system operation.

## III. SWB-BASED BUOY SYSTEM IMPLEMENTATION

### A. DEGRADATION PREDICTION & FAULT DETECTION

Fig. 4 presents the operational principle of the proposed variance-based scheme for SWB degradation prediction and fault detection. The SWB's operational status is monitored, and also it is protected from major functional risks of overcharge and undercharge, which provide a way to predict the SWB performance degradation. The proposed buoy system obtains the SOC of the SWB by including two current sensing circuits which are designed to measure current flows at both input and output interfaces of the SWB. They continuously measure two kinds of current flows that are charged into the SWB and discharged from it respectively.

$$Q_{charge} = \int_0^T I_{charge} * t_{charge} \tag{1}$$

$$Q_{discharge} = \int_0^T I_{discharge} * t_{discharge} \tag{2}$$

Equation (1) and (2) represent two accumulated charge quantities calculated from the charged current and the discharged current in the SWB, where $I_{charge}$ and $I_{discharge}$ are measured charge/discharge currents, $t_{charge}$ and $t_{discharge}$ are their charge/discharge times, and T represents a time period for the SWB operation. Measured current amount is converted into a voltage through a small resistance ($R_{sense}$) inside the current-sensing circuit. It is sampled and converted to a digital data by the ADC inside the MCU, and then further processed to estimate the CCSOC information of the SWB.

$$Q'_{charge} = \sum_{n=1}^{m} I_{charge}[n] * R_{sense} * t_{sample} \tag{3}$$

$$Q'_{discharge} = \sum_{n=1}^{m} I_{discharge}[n] * R_{sense} * t_{sample} \tag{4}$$

Equation (3) and (4) are obtained by multiplying the accumulated charge data by $R_{sense}$, where $I_{charge}[n]$ and $I_{discharge}[n]$ represent discrete current data to be sampled by the ADC. $t_{sample}$ means the calculation period. n is the number of calculation trials and m is the total number of calculations. Then, the MCU calculates the effective charge amount inside the SWB, and then the CCSOC information is obtained as follows:

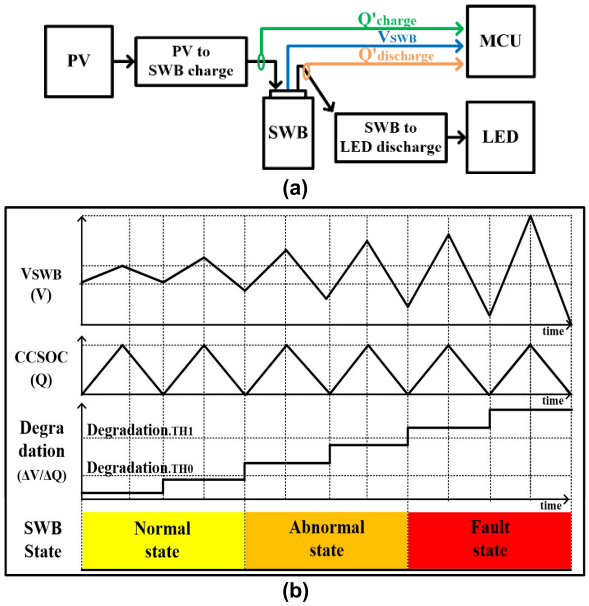


**FIGURE 4.** Operational principle of SWB degeneration prediction and fault detection: (a) block diagram and (b) operational waveforms.

$$Q'_{battery} = Q'_{charge} - Q'_{discharge} \tag{5}$$

$$Q_{battery} = Q'_{battery} * \frac{1}{R_{sense}} \tag{6}$$

Besides this CCSOC information, the cell voltage of the SWB ($V_{SWB}$) is additionally measured for the proposed hybrid estimation of degradation prediction and fault detection. As shown in Fig. 4(b), the swing amplitude of $V_{SWB}$ when it is periodically charged or discharged with the same total amount of charge varies as the aging process proceeds [38]. The aging process in the SWB is supposed to cause the increment of $V_{SWB}$'s variance amplitude even with the same change of CCSOC. Therefore, this hybrid monitoring of the $V_{SWB}$'s variance together with the CCSOC is supposed to estimate the performance degradation degree of the SWB. This SWB degradation estimation is utilized to recognize three degradation progress states of normal, abnormal, and fault.

$$\begin{aligned} Degradation_{charge} &= \frac{\Delta V_{SWB}}{\Delta Q_{.effective-charge.SWB}} \\ &= \frac{V_{SWB}[n] - V_{SWB}[n-1]}{Q_{charge}[n] - Q_{charge}[n-1]} \end{aligned} \tag{7}$$

$$\begin{aligned} Degradation_{discharge} &= \frac{\Delta V_{SWB}}{\Delta Q_{.effective-discharge.SWB}} \\ &= \frac{V_{SWB}[n] - V_{SWB}[n-1]}{Q_{discharge}[n] - Q_{discharge}[n-1]} \end{aligned} \tag{8}$$

The degradation is estimated as the $V_{SWB}$ variance normalized by the effective amount of charge or discharge, where $\Delta Q_{.effective\text{-}charge.SWB}$ and $\Delta Q_{.effective\text{-}discharge.SWB}$ represent the effective charge and discharge amounts, and $\Delta V_{SWB}$ means the swing amplitude or variance of the $V_{SWB}$. Then, these instant measurements are periodically averaged as follows:

$$Degrade_{ave.charge} = \sum_{n=1}^{N} \frac{Degradation_{charge}}{N} \quad (9)$$

$$Degrade_{ave.discharge} = \sum_{n=1}^{N} \frac{Degradation_{discharge}}{N} \quad (10)$$

Fig. 5 shows detailed implementation flow chart of SOC monitoring, battery degradation prediction, and fault detection. While the buoy system monitors the SOC of the SWB, if the CCSOC is less than $CCSOC_{.min}$, the undercharge protection (UCP) is activated. When the CCSOC is greater than $CCSOC_{.max}$, the overcharge protection (OCP) is turned on to disconnect the PV cell from the SWB. The normal operation corresponds to the state when the CCSOC is kept between $CCSOC_{.min}$ and $CCSOC_{.max}$. To remove the accumulation error and perform hydrogen evolution reaction (HER) along with the ORR reaction, the CCSOC is resetted when the $V_{SWB}$ goes below the $V_{RESET.TH}$. The total capacity is adaptively adjusted by replacing CCSOC.max by subtracting the present CCSOC from original CCSOC.max data. The LED lighting is activated if $V_{PV}$ is less than $V_{PV.TH}$ for some period, where the PV cell is utilized to work as an illumination sensor. In the meanwhile, the proposed variance-based degradation prediction algorithm is performed to monitor the aging progress of the SWB. The average degradation (Degrade.ave) is compared with two critical values of $Degradation_{.TH0}$ and $Degradation_{.TH1}$, and then three degradation states of normal, abnormal, and fault are determined. In case of the fault state, the UPS works as the power source of the buoy system instead of the SWB, and its wireless application platform notifies to the user that the SWB needs to be replaced.

### B. MULTIPLE POWER OPTIMIZATION CAPABILITIES

The proposed buoy system utilizes the CCSOC method to manage the SWB and adopts multiple power optimization schemes to achieve its sustainable self-powered operation. While the SWB drives the system in the normal mode, both save and UPS modes are selectively activated depending on the CCSOC level. When the CCSOC is less than a certain level, the save mode would expand the operation time by adjusting the LED lighting. If the CCSOC becomes less than $CCSOC_{.min}$, the UPS mode is activated, that is, the SWB is replaced with the UPS. As shown in Fig. 6, the power delivery path consists of four major blocks, where Block (1)-(4) represent a PV to SWB circuit, a SWB to LED circuit, a PV to UPS circuit, and a DC-DC converter for the MCU. Additional auxiliary switches are used to deliver the

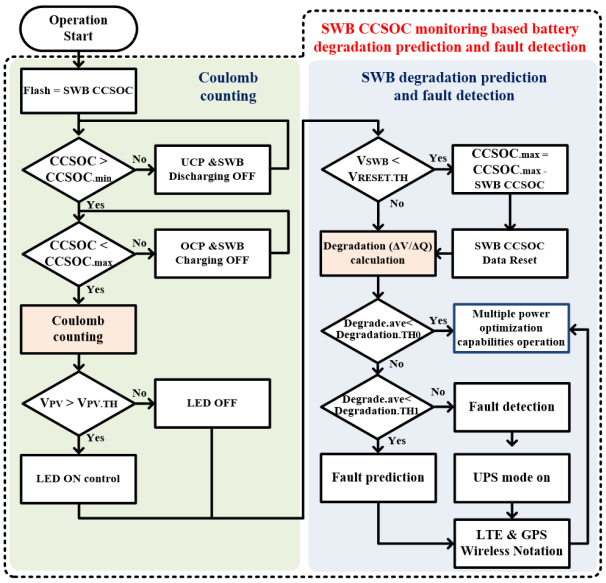


**FIGURE 5.** Detailed flow chart of CCSOC monitoring, SWB degradation prediction and fault detection.

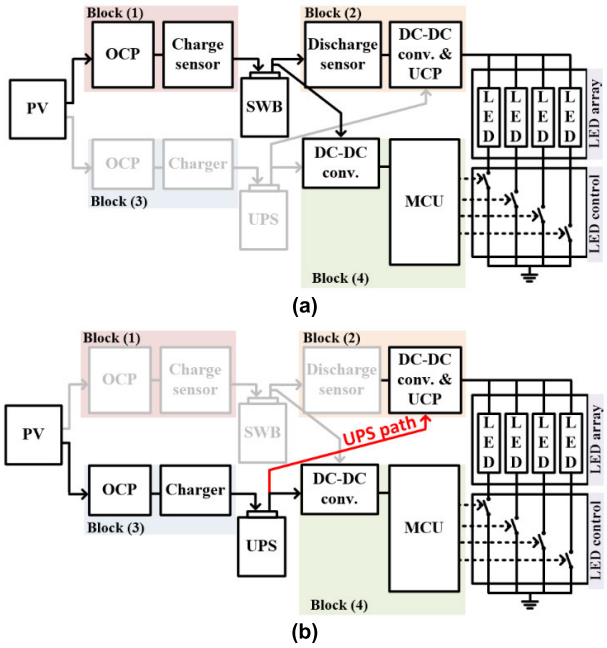


**FIGURE 6.** Power delivery configurations (a) in normal and save modes and (b) in UPS mode.

energy from either the SWB or the UPS. The MCU receives five control data of $V_{PV}$, $V_{UPS}$, $V_{SWB}$, $Q_{charge+}$, and $Q_{charge-}$. Based on these data, the LED lighting is adjusted adaptively, and the system operation mode is properly optimized. Fig. 6(a) shows the normal-mode operation with SWB-based power delivery that every power is provided by the SWB. Fig. 6(b) shows the UPS-mode operation where the power delivery path is switched to the UPS, instead of the SWB.

Fig. 7 presents the concept of the three-step LED lighting control in the SWB save mode, which corresponds to LED array control, LED PWM control, and LED PFM control.

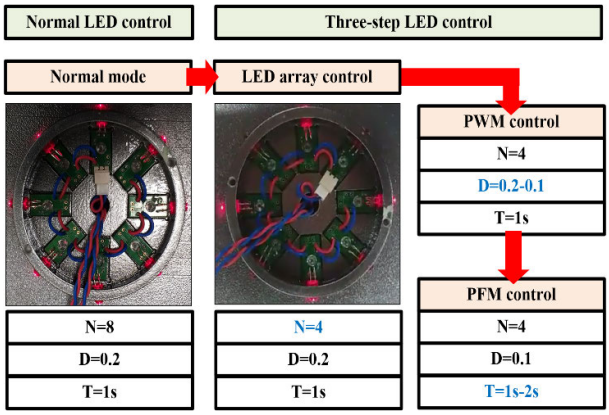


**FIGURE 7.** Three-step LED lighting control.

If the CCSOC of the SWB is slightly lower than the normal state ($Q_{SWB.TH3}$), the LED array control reduces the number of LED lights. Then, the power consumption is saved by the reduced number of LEDs while control period and duty are unchanged. When the CCSOC goes under the $Q_{SWB.TH2}$, their control duty is reduced by the LED PWM control while their lighting period is kept constant. However, in order to recognize the light of the LED, a minimal on-duty is required, which gives a limit for reducing the on-time duty below a certain level. Therefore, if the CCSOC of the SWB is less than $Q_{SWB.TH1}$, the LED lighting period is controlled by the LED PFM control for further power saving. Fig 8 shows the operational flow chart of CCSOC-based multiple power optimization schemes. Since the CCSOC information determines detailed operating conditions, the threshold CCSOC values for their decisions are set inside the algorithm. Depending on real-time CCSOC monitoring results, the operation mode and the LED light control are adaptively optimized. After this power optimization process, the system loops back to the SWB degradation prediction algorithm.

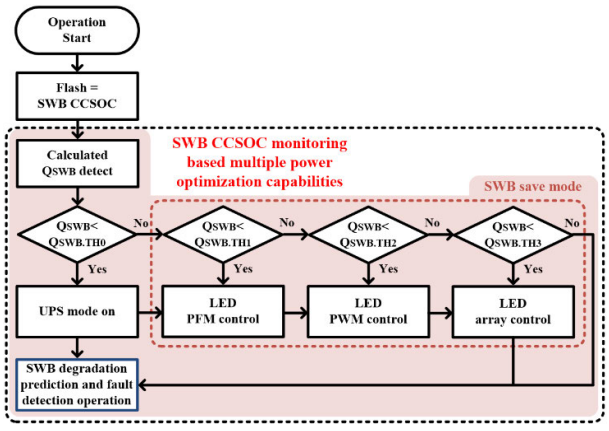


**FIGURE 8.** Flow chart of CCSOC-based multiple power optimizations.

## IV. EXPERIMENTAL RESULTS

### A. BUOY SYSTEM PROTOTYPE

Fig. 9 shows a prototype implementation of the SWB-based marine buoy system which consists of the SWB, the PV cell,

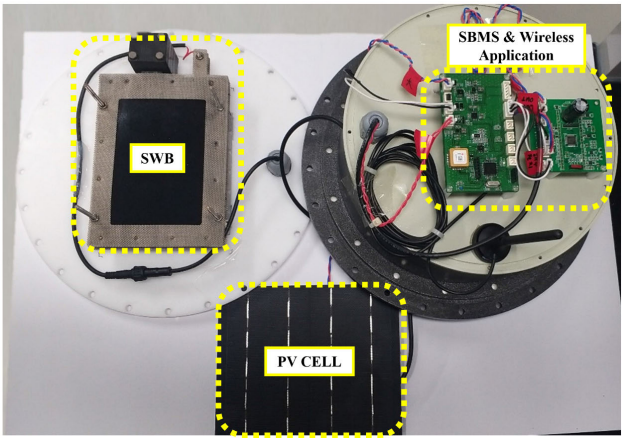


**FIGURE 9.** Photograph of the SWB-based marine buoy system.

and their control circuit module. The circuit module is composed of a SWB management system (SBMS) and a wireless application module. The SBMS includes a power delivery circuit and a SWB algorithm controller. Additionally, an LED array is installed at the center of the buoy. The wireless application module provide two functions of global positioning system (GPS) and LTE communication, whose antenna is installed near the wireless application module. Since SWB cells are used as being immersed under the sea, they are located at the bottom of the buoy. In the SBMS, a SWB management algorithm for the CCSOC is implemented with an ARM-based MCU (STM32L4) and an operational amplifier (INA210) for current-shunt monitoring, where the ADC inside the MCU is utilized at 20-ms sampling period. Additionally, a DC-DC converter (TPS63030) and switches of MOSFET (IRF7507) and BJT (BC817K-25R) types are included for power management and LED light control. In addition, a 4700-uF capacitor is included to provide stable power transition during self-powered buoy operation when the power source is changed from UPS to the SWB. This large capacitor guarantees the operation of the MCU for the transitional period, allowing that the CCSOC data are stably stored in flash memory in the MCU. The wireless application module consists of a GPS module and an LTE cellular modem. Since its instant power consumption is relatively large, the UPS is utilized for its power source instead of the SWB. The battery status data including $V_{SWB}$, $V_{UPS}$, CCSOC and the degree of performance degradation are wirelessly transmitted to a server every six hours.

The SWB consists of three components, that is, an anode in a non-aqueous electrolyte, the seawater with a cathode current collector, and a solid electrolyte. The anode plays a significant role in determining SWB energy capacity since it stores Na+ ions which are harvested from the seawater in the charging process. The seawater infinitely supplies Na+ ions for anodic reactions during the charging process, and its dissolved oxygen works as an oxidant during the discharging. With sufficient Na+ ions and dissolved oxygen, the seawater

acts as the sole active cathode material. Lastly, the solid electrolyte separates two electrodes by positioning between them. Only $Na^+$ ions are transported and returned through the solid electrolyte during charging or discharging processes. In this work, three 450-mAh SWB cells were used in parallel. It is designed to provide the current up to 150 mA and the total capacity of 1,350 mAh. The PV cell units are used as a series and parallel connection. The PV cell is designed to generate 4.0 V using a series connection. In a parallel connection, the current up to 150 mA can be charged to the SWB under the best weather condition.

Fig. 10 shows the measurement setup of the SWB with the BMS and charger. The voltage profile of the SWB is recorded via a Data Logger (GL2000) and the coulomb counting is proceeded with a charger (VSP-300) and monitored through a MCU Keil program. Fig. 11 shows two typical charge and discharge profiles of the SWB with 100-mAh capacity. As inherent characteristics of the SWB, the OCV of the SWB tends to return to a constant voltage which is not dependent on the SOC. Fig. 11(a) shows its measured waveform, where the SWB was charged with constant 30-mA current and then charging operation was stopped at the full charge condition. Until $T_1$, which is around 15 hours, the $V_{SWB}$ increased during the process of charging. However, after fully charged, the $V_{SWB}$ returned to around 3.2 V again. Fig. 11(b) shows another measured waveform, where the SWB was discharged with the same 30-mA current for the same time. As the SWB becomes discharged, the $V_{SWB}$ decreases until $T_2$, which is close to $T_1$, but the OCV returned to 3.2 V when the discharging was stopped. As a result, since the regression to a stable OCV took very long time, it was difficult to estimate SOC through the OCV. Even if the $V_{SWB}$ was measured in real time, accurate SOC estimation was impossible. Because of these inherent characteristics, the CCSOC estimation was necessary to perform reliable SOC estimation for the SWB.

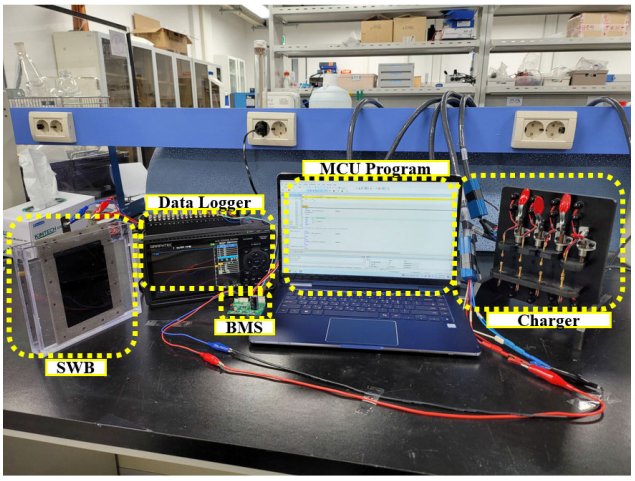


**FIGURE 10.** Measurement setup of the SWB with the BMS and charger.

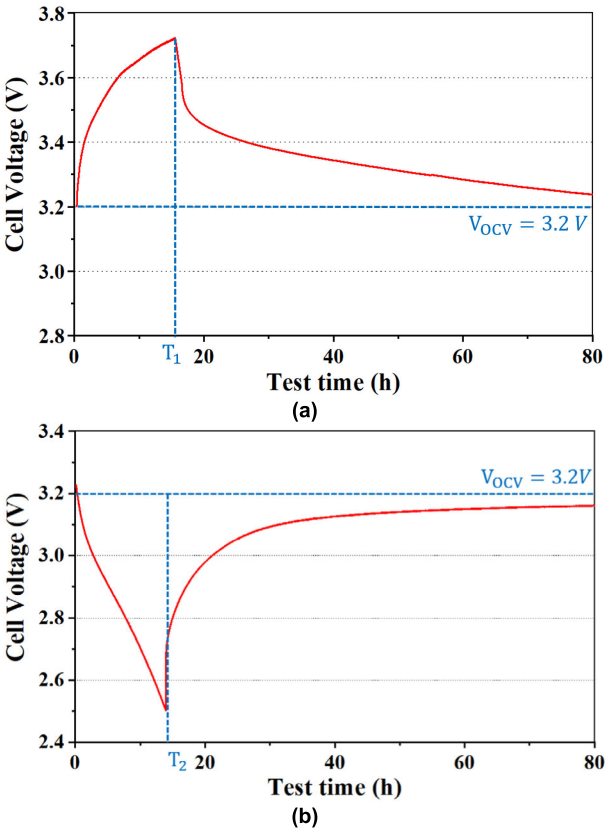


**FIGURE 11.** Charge/discharge profile of SWB during a one cycle: (a) charging profile of SWBs, (b) discharging profile of SWB.

### B. SWB DEGRADATION PREDICTION

Fig. 12 shows measurement results of $V_{SWB}$ and SOC with 100-mAh SWB during the CCSOC estimation. Fig. 12(a) shows measured waveforms of $V_{SWB}$ and SOC at periodic balanced charging/discharging conditions. In this periodic process, constant current charging was proceeded with the 30-mA current until the CCSOC of SWB reached to 100 %, starting from 10 %. And the discharging was started when the SWB was fully charged. The total capacity of the SWB in this experiment was 100 mAh. Fig. 12(b) shows measured waveforms of $V_{SWB}$ and SOC at periodic unbalanced charging/discharging condition with the SWB charging process. The charging proceeded with 30-mA current for 3 hours and the discharging proceeded with 24-mA current for 3 hours. After every cycle of charging and discharging, the average SOC increased closely to 100 %. During this experiment, $V_{SWB}$ and SOC data were monitored by the CCSOC estimation until the full-charge condition. As shown in Fig 12, when sufficient rest time after charging or discharging processes was not guaranteed, the $V_{SWB}$ was not returned to a certain level. And, the saturated OCV was not clearly proportional to the SOC. However, although the $V_{SWB}$ is independent of the SOC, the slope of $V_{SWB}$ can be a major indicator of the SWB performance degradation. The degree of the performance degradation can be evaluated through how much the VSWB has changed with respect to actual charging amount.

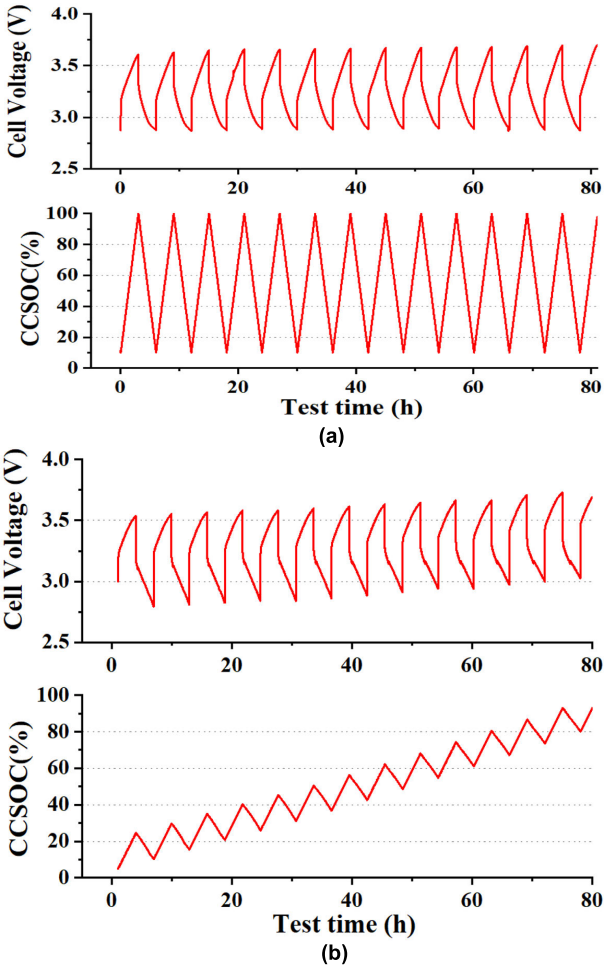


**FIGURE 12.** Measured cell voltage and SOC of SWBs based on the CCSOC estimation (a) at periodic balanced charging/discharging condition and (b) at periodic unbalanced charge/discharge condition with SWB charging process.

The indicator also can be used as estimating the degradation degree in real time even when charging and discharging amounts are not constant.

Fig. 13 shows measurement results of performance degradation prediction and fault detection based on the CCSOC. To obtain extreme profiles of the degradation, the experiment was performed with 10-mA constant charging and discharging condition. The SWB was 50-mAh capacity with initial normal state. In Fig. 12(a), the measured $V_{SWB}$ and the degradation degree are shown. The $V_{SWB}$ was periodically monitored by the MCU with every 20 ms. The lower figure on the degradation was rescaled to effectively represent the SWB state in the y-axis of the graph.

$$Degradation = \frac{Degrade_{ave}}{Degradation_{Max}} * 100 \quad (11)$$

$$Degradation_{Max} = V_{Range.Max}/Q_{battery.Max} \quad (12)$$

In equation (11), Degradation is a percentage value of $Degrade_{.ave}$ over $Degradation_{Max}$. The $Degrade_{.ave}$ is substituted as $Degrade_{.ave.charge}$ or $Degrade_{.ave.discharge}$ depending

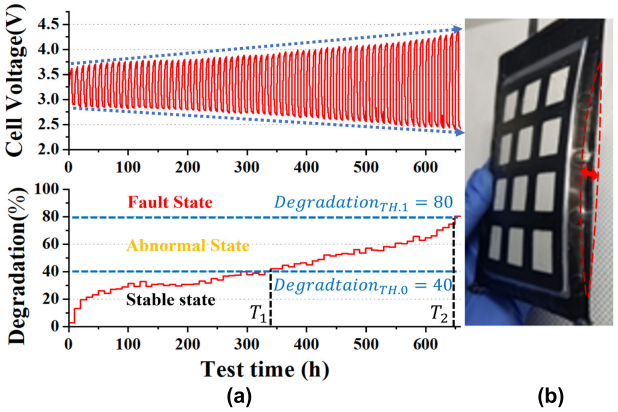


**FIGURE 13.** Measurement results of based SWB performance degradation prediction and fault detection based on the CCSOC estimation: (a) Measured cell voltage and degradation figure, (b) Photo of the SWB in fault state.

on the operating condition of charge or discharge. Equation (12) shows a coefficient to represent the maximum value of the degradation, where $V_{Range.Max}$ is the maximum allowable voltage range of the circuit and the SWB, and $Q_{battery.Max}$ is the maximum capacity of the SWB. Through long-term experiments, the SWB which was initially in the normal state went to the degradation state. Around $T_1$, which is 340 hours, the degradation crossed the first critical value of $Degradation_{TH,0}$, which means that the status of the SWB was changed to the abnormal state. Around $T_2$, which is 640 hours, the figure of degradation crossed the second critical value of $Degradation_{TH,1}$, which means that the status of the SWB was changed to the fault state. During this experiment, overall status of the SWB was periodically transmitted to an LTE server through the wireless application module. Especially, when the fault state was detected, it aroused the warning message that the SWB needs to be replaced. Fig. 12(b) shows the photo of the swollen SWB. As the degradation got worse, the SWB became swelled. For stable operation, the SWB required more charging voltage, lower discharging voltage, which leaded to low battery efficiency.

### C. MULTIPLE POWER OPTIMIZATION

Fig. 14(a) shows a measured pie chart on the lifetime of the SWB in the save mode and the UPS mode. The system operates in the normal mode under the total CCSOC condition from 100 % to 50 %. The number of lighting LEDs was eight, the lighting period was 1 s, and the lighting on-duty was 0.2 s. If the CCSOC becomes below 50 %, the system operation changes to the SWB save mode. The SWB save mode operated as a kind of power-saving mode by applying the three-step LED control depending on the CCSOC condition. In the CCSOC condition from 40 % to 50 %, the system operates as step 1, which activates the LED array control. In this case, the number of lighting LEDs is reduced to four, the lighting period and the lighting on-duty are kept as the same. In the CCSOC

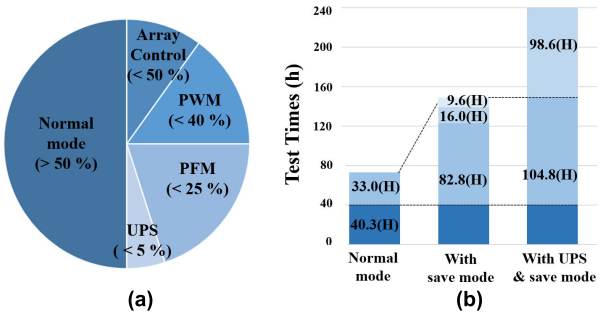


**FIGURE 14.** Measured SWB lifetime in SWB save mode and UPS technique: (a) SWB save mode and UPS technique operation depending on CCSOC, (b) comparison of SWB lifetime in normal mode, SWB save mode, and UPS technique.

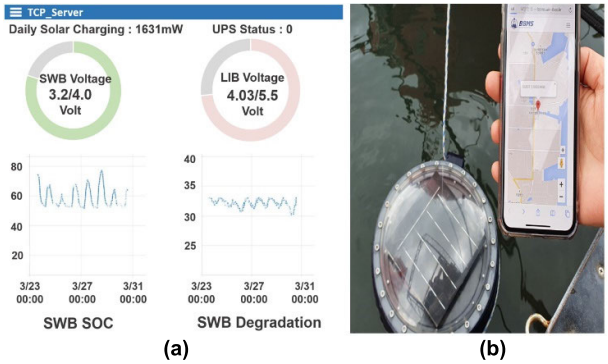


**FIGURE 15.** Mobile application platform of battery status and location data monitoring of wireless buoy system: (a) battery status monitoring using LTE and (b) buoy location monitoring using GPS.

between 25 % and 40 %, the system operates as step 2, which uses the LED array control and the LED PWM control. The lighting on-duty is changed from 0.2 s to 0.1 s, and others were kept as the same. Next, in step 3 which corresponds to the CCSOC from 5 % to 25 %, the system utilizes the LED array control, the LED PWM control, and the LED PFM control. In the step 3, the lighting period is modulated from 1 s to 2 s. Nevertheless, when the CCSOC dropped under the 5 %, the UPS substitute the SWB to prevent from being overcharged.

Fig. 14(b) shows the comparison of the SWB lifetimes in the normal mode, the SWB save mode, and the UPS mode, where all experiments were conducted under the same SWB conditions. The initial condition of the SWBs was equally full charged. The capacity of the SWB used in the experiment was 1350 mAh and the stable current range was less than 150 mA. The maximum power was 600 mW. For the normal mode, the SWB save mode, and the SWB save mode with UPS mode, the operation time corresponded to 73.3 hours, 148.7 hours, and 243.7 hours respectively. The proposed three-step LED control saved the energy of the SWB and extended the usage time further with the UPS technique. Consequently, the system with the SWB save mode and the UPS mode was operated longer as much as 170.4 hours than the normal mode.

### D. WIRELESS PLATFORM

Fig. 15 shows the mobile platform for battery status and location data monitoring of the proposed wireless buoy system prototype. Fig. 15(a) shows the battery status monitored by the LTE, where $V_{SWB}$, $V_{UPS}$, SOC status, degradation degree were periodically updated. Especially, the SWB status graphs including the SOC and the performance degradation were refreshed every 6 hours. Since the power consumption of the GPS and the LTE was relatively large, the wireless application module operated for a short time over a long period and worked as a standby mode for the rest of time. Fig. 15(b) shows a photo of the GPS operation that was implemented at a nearby ocean, where the buoy geometric information was available on the smartphone. Table 1 represents the performance summary of the proposed work compared with other recent works.

**TABLE 1.** Performance summary and comparison with other recent work.

| | This work | [25] | [26] | [27] | [28] | [29] | [30] |
|---|---|---|---|---|---|---|---|
| Batttery | SWB | LIB | LIB | LIB | LIB | LIB | LIB |
| SOH Estimation Method | Variance-based detection | CC | OCV | OCV | OCV (KF) | CC (Fuzzy logic) | CC (ANNs) |
| Over/Under Charge Protection | YES | YES | YES | No | YES | No | YES |
| Over/Under Voltage Protection | YES | No | No | YES | No | No | No |
| SOC monitoring | YES | YES | YES | YES | YES | YES | YES |
| Degrdation/SOH monitoring | YES | YES | YES | YES | YES | YES | No |
| Real time (SOH) | YES | No | No | No | YES | YES | No |
| Mode of operation | Online/Offline | Online | Online | offline | online | online | online |
| Estimated Error | <2.5% | < 8.9% | <5% in most of the cases | <3% | <5% | <9.2% | <0.5% |

## V. CONCLUSION

This paper presented the intelligent SWB-based wireless marine buoy system, where its battery degradation prediction and multiple power optimization were proposed and functionally verified. The performance degradation prediction scheme of the SWB was proposed based on the variance-based detection method, which protected the SWB from functional risks of overcharge and undercharge. Based on the proposed SOC and SOH method, PV-based self-powered operation was optimized through two proposed power schemes of multiple power management and three-step LED control. Its wireless buoy prototype was designed to deliver buoy information on battery status and geometric location to the LTE server, implementing a mobile service platform for periodic real-time monitoring of the intelligent marine buoys.

## ACKNOWLEDGMENT

*(Jeonghoon Cho and Myeong Woo Kim contributed equally to this work.)*

## REFERENCES

[1] J. H. Kim, S. M. Hwang, I. Hwang, J. Han, J. H. Kim, Y. H. Jo, K. Seo, Y. Kim, and J. S. Lee, "Seawater-mediated solar-to-sodium conversion by bismuth vanadate photoanode-photovoltaic tandem cell: Solar rechargeable seawater battery," *iScience*, vol. 19, pp. 232–243, Sep. 2019, doi: 10.1016/j.isci.2019.07.024.

[2] Y. Kim, S. M. Hwang, H. Yu, and Y. Kim, "High energy density rechargeable metal-free seawater batteries: A phosphorus/carbon composite as a promising anode material," *J. Mater. Chem. A*, vol. 6, no. 7, pp. 3046–3054, 2018, doi: 10.1039/C7TA10668H.

[3] J.-K. Kim, F. Mueller, H. Kim, S. Jeong, J.-S. Park, S. Passerini, and Y. Kim, "Eco-friendly energy storage system: Seawater and ionic liquid electrolyte," *ChemSusChem*, vol. 9, no. 1, pp. 42–49, Jan. 2016, doi: 10.1002/cssc.201501328.

[4] A. Manthiram, "A reflection on lithium-ion battery cathode chemistry," *Nature Commun.*, vol. 11, no. 1, pp. 1–9, Dec. 2020, doi: 10.1038/s41467-020-15355-0.

[5] A. Manthiram, "An outlook on lithium ion battery technology," *ACS Central Sci.*, vol. 3, no. 10, pp. 1063–1069, Oct. 2017, doi: 10.1021/acscentsci.7b00288.

[6] L. Zhang, X. Hu, Z. Wang, J. Ruan, C. Ma, Z. Song, D. G. Dorrell, and M. G. Pecht, "Hybrid electrochemical energy storage systems: An overview for smart grid and electrified vehicle applications," *Renew. Sustain. Energy Rev.*, vol. 139, Apr. 2021, Art. no. 110581, doi: 10.1016/j.rser.2020.110581.

[7] E. A. Olivetti, G. Ceder, G. G. Gaustad, and X. Fu, "Lithium-ion battery supply chain considerations: Analysis of potential bottlenecks in critical metals," *Joule*, vol. 1, no. 2, pp. 229–243, Oct. 2017, doi: 10.1016/j.joule.2017.08.019.

[8] S. Park, B. SenthilKumar, K. Kim, S. M. Hwang, and Y. Kim, "Salt-water as the energy source for low-cost, safe rechargeable batteries," *J. Mater. Chem. A*, vol. 4, no. 19, pp. 7207–7213, 2016, doi: 10.1039/C6TA01274D.

[9] Y. J. Lim, J. Han, H. W. Kim, Y. Choi, E. Lee, and Y. Kim, "An epoxy-reinforced ceramic sheet as a durable solid electrolyte for solid state na-ion batteries," *J. Mater. Chem. A*, vol. 8, no. 29, pp. 14528–14537, Jul. 2020, doi: 10.1039/D0TA06024K.

[10] L. Zhang, W. Fan, Z. Wang, W. Li, and D. U. Sauer, "Battery heating for lithium-ion batteries based on multi-stage alternative currents," *J. Energy Storage*, vol. 32, Dec. 2020, Art. no. 101885, doi: 10.1016/j.est.2020.101885.

[11] Y. Kim, G.-T. Kim, S. Jeong, X. Dou, C. Geng, Y. Kim, and S. Passerini, "Large-scale stationary energy storage: Seawater batteries with high rate and reversible performance," *Energy Storage Mater.*, vol. 16, pp. 56–64, Jan. 2019, doi: 10.1016/j.ensm.2018.04.028.

[12] M. Ligaray, N. Kim, S. Park, J.-S. Park, J. Park, Y. Kim, and K. H. Cho, "Energy projection of the seawater battery desalination system using the reverse osmosis system analysis model," *Chem. Eng. J.*, vol. 395, Sep. 2020, Art. no. 125082, doi: 10.1016/j.cej.2020.125082.

[13] Y. Zhang, S. T. Senthilkumar, J. Park, J. Park, and Y. Kim, "A new rechargeable seawater desalination battery system," *Batteries Supercaps*, vol. 1, no. 1, pp. 6–10, Jul. 2018, doi: 10.1002/batt.201800012.

[14] S. M. Hwang, J. Park, Y. Kim, W. Go, J. Han, Y. Kim, and Y. Kim, "Rechargeable seawater batteries—From concept to applications," *Adv. Mater.*, vol. 31, no. 20, May 2019, Art. no. 1804936, doi: 10.1002/adma.201804936.

[15] Y. Kim, A. M. Harzandi, J. Lee, Y. Choi, and Y. Kim, "Design of large-scale rectangular cells for rechargeable seawater batteries," *Adv. Sustain. Syst.*, vol. 5, no. 1, Jan. 2021, Art. no. 2000106, doi: 10.1002/adsu.202000106.

[16] T.-U. Wi, C. Lee, M. F. Rahman, W. Go, S. H. Kim, D. Y. Hwang, S. K. Kwak, Y. Kim, and H.-W. Lee, "Chemical stability and degradation mechanism of solid electrolytes/aqueous media at a steady state for long-lasting sodium batteries," *Chem. Mater.*, vol. 33, no. 1, pp. 126–135, Jan. 2021, doi: 10.1021/acs.chemmater.0c03022.

[17] N. Kim, J.-S. Park, A. M. Harzandi, K. Kishor, M. Ligaray, K. H. Cho, and Y. Kim, "Compartmentalized desalination and salination by high energy density desalination seawater battery," *Desalination*, vol. 495, Dec. 2020, Art. no. 114666, doi: 10.1016/j.desal.2020.114666.

[18] Y. Kim, J. Jung, H. Yu, G. Kim, D. Jeong, D. Bresser, S. J. Kang, Y. Kim, and S. Passerini, "Sodium biphenyl as anolyte for sodium–seawater batteries," *Adv. Funct. Mater.*, vol. 30, no. 24, Jun. 2020, Art. no. 2001249, doi: 10.1002/adfm.202001249.

[19] S. Lee, I. Y. Cho, D. Kim, N. K. Park, J. Park, Y. Kim, S. J. Kang, Y. Kim, and S. Y. Hong, "Redox-active functional electrolyte for high-performance seawater batteries," *ChemSusChem*, vol. 13, no. 9, pp. 2220–2224, May 2020, doi: 10.1002/cssc.201903564.

[20] J. Park, J.-S. Park, S. T. Senthilkumar, and Y. Kim, "Hybridization of cathode electrochemistry in a rechargeable seawater battery: Toward performance enhancement," *J. Power Sources*, vol. 450, Feb. 2020, Art. no. 227600, doi: 10.1016/j.jpowsour.2019.227600.

[21] S. Park, Z. Khan, T. J. Shin, Y. Kim, and H. Ko, "Rechargeable Na/Ni batteries based on the $Ni(OH)_2$/NiOOH redox couple with high energy density and good cycling performance," *J. Mater. Chem. A*, vol. 7, no. 4, pp. 1564–1573, Jan. 2019, doi: 10.1039/C8TA10830G.

[22] J. Kim, J. Shin, C. Chun, and B. H. Cho, "Stable configuration of a Li-ion series battery pack based on a screening process for improved voltage/SOC balancing," *IEEE Trans. Power Electron.*, vol. 27, no. 1, pp. 411–424, Jan. 2012, doi: 10.1109/TPEL.2011.2158553.

[23] S. T. Senthilkumar, W. Go, J. Han, L. P. T. Thuy, K. Kishor, Y. Kim, and Y. Kim, "Emergence of rechargeable seawater batteries," *J. Mater. Chem. A*, vol. 7, no. 40, pp. 22803–22825, Oct. 2019, doi: 10.1039/C9TA08321A.

[24] W. Lee, J. Park, J. Park, S. J. Kang, Y. Choi, and Y. Kim, "Identifying the mechanism and impact of parasitic reactions occurring in carbonaceous seawater battery cathodes," *J. Mater. Chem. A*, vol. 8, no. 18, pp. 9185–9193, May 2020, doi: 10.1039/D0TA02913K.

[25] K. S. Ng, C.-S. Moo, Y.-P. Chen, and Y.-C. Hsieh, "Enhanced coulomb counting method for estimating state-of-charge and state-of-health of lithium-ion batteries," *Appl. Energy*, vol. 86, no. 9, pp. 1506–1511, Sep. 2009, doi: 10.1016/j.apenergy.2008.11.021.

[26] W. Waag, C. Fleischer, and D. U. Sauer, "Adaptive on-line prediction of the available power of lithium-ion batteries," *J. Power Sources*, vol. 242, pp. 548–559, Nov. 2013, doi: 10.1016/j.jpowsour.2013.05.111.

[27] Z. Wang, J. Ma, and L. Zhang, "State-of-health estimation for lithium-ion batteries based on the multi-island genetic algorithm and the Gaussian process regression," *IEEE Access*, vol. 5, pp. 21286–21295, 2017, doi: 10.1109/ACCESS.2017.2759094.

[28] J. Kim, S. Lee, and B. H. Cho, "Complementary cooperation algorithm based on DEKF combined with pattern recognition for SOC/capacity estimation and SOH prediction," *IEEE Trans. Power Electron.*, vol. 27, no. 1, pp. 436–451, Jan. 2012, doi: 10.1109/TPEL.2011.2158554.

[29] M. Landi and G. Gross, "Measurement techniques for online battery state of health estimation in vehicle-to-grid applications," *IEEE Trans. Instrum. Meas.*, vol. 63, no. 5, pp. 1224–1234, May 2014, doi: 10.1109/TIM.2013.2292318.

[30] M. A. Hannan, M. S. H. Lipu, A. Hussain, M. H. Saad, and A. Ayob, "Neural network approach for estimating state of charge of lithium-ion battery using backtracking search algorithm," *IEEE Access*, vol. 6, pp. 10069–10079, 2018, doi: 10.1109/ACCESS.2018.2797976.

[31] Q. Wang, Z. Wang, L. Zhang, P. Liu, and Z. Zhang, "A novel consistency evaluation method for series-connected battery systems based on real-world operation data," *IEEE Trans. Transport. Electrific.*, vol. 7, no. 2, pp. 437–451, Jun. 2021, doi: 10.1109/TTE.2020.3018143.

[32] A. H. M. A. Helmi, M. M. Hafiz, and M. S. B. S. Rizam, "Mobile buoy for real time monitoring and assessment of water quality," in *Proc. IEEE Conf. Syst., Process Control (ICSPC)*, Dec. 2014, pp. 19–23, doi: 10.1109/SPC.2014.7086223.

[33] B. Kesavakumar, M. ArulMuthiah, S. Elango, D. Gowthaman, P. Kaliyaperumal, P. Senthilkumar, R. Sridharan, and R. Venkatesan, "Design of optimal power source for NIOT offshore moored buoy system," in *Proc. Ocean Electron. (SYMPOL)*, 2013, pp. 189–195, doi: 10.1109/SYMPOL.2013.6701929.

[34] Y. Li, Q. Guo, M. Huang, X. Ma, Z. Chen, H. Liu, and L. Sun, "Study of an electromagnetic ocean wave energy harvester driven by an efficient swing body toward the self-powered ocean buoy application," *IEEE Access*, vol. 7, pp. 129758–129769, 2019, doi: 10.1109/ACCESS.2019.2937587.

[35] M. Magno, T. Polonelli, L. Benini, and E. Popovici, "A low cost, highly scalable wireless sensor network solution to achieve smart LED light control for green buildings," *IEEE Sensors J.*, vol. 15, no. 5, pp. 2963–2973, May 2015, doi: 10.1109/JSEN.2014.2383996.

[36] S. Matta and S. M. Mahmud, "An intelligent light control system for power saving," in *Proc. 36th Annu. Conf. IEEE Ind. Electron. Soc. (IECON)*, Nov. 2010, pp. 3316–3321, doi: 10.1109/IECON.2010.5675331.

[37] M.-S. Pan, L.-W. Yeh, Y.-A. Chen, Y.-H. Lin, and Y.-C. Tseng, "A WSN-based intelligent light control system considering user activities and profiles," *IEEE Sensors J.*, vol. 8, no. 10, pp. 1710–1721, Oct. 2008, doi: 10.1109/JSEN.2008.2004294.
[38] J. Han, S. Lee, C. Youn, J. Lee, Y. Kim, and T. Choi, "Hybrid photoelectrochemical-rechargeable seawater battery for efficient solar energy storage systems," *Electrochimica Acta*, vol. 332, Feb. 2020, Art. no. 135443, doi: 10.1016/j.electacta.2019.135443.

**JEONGHOON CHO** was born in Jeonju, South Korea, in 1993. He received the B.S. degree in electrical engineering from Ulsan National Institute of Science and Technology (UNIST), Ulsan, South Korea, in 2018, where he is currently pursuing the M.S./Ph.D. combined program. His research interests include analog/mixed-signal integrated circuits and power management integrated circuits.

**MYEONG WOO KIM** was born in Daegu, South Korea, in 1994. He received the B.S. degree in electrical engineering from Ulsan National Institute of Science and Technology (UNIST), Ulsan, South Korea, in 2017, where he is currently pursuing the M.S./Ph.D. combined program. His research interests include analog/mixed-signal integrated circuits and power management integrated circuits.

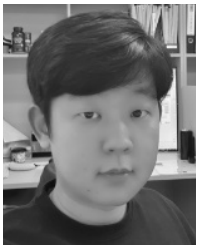

**YOUNGJIN KIM** received the M.S. degree from Changwon National University, Changwon, South Korea, in 2016. He is currently pursuing the Ph.D. degree in energy engineering with Ulsan National Institute of Science and Technology (UNIST), under the supervision of Prof. Youngsik Kim. His research interests include electrochemical cell systems and its applications.

**JEONG-SUN PARK** received the Ph.D. degree in energy engineering from Ulsan National Institute of Science and Technology (UNIST), in 2020, under the supervision of Prof. Youngsik Kim. He is currently a Chief Technology Officer (CTO) at 4TOONE Corporation, an energy solution company. He conducted research in the electrode and cell design, optimization of cell components, stack engineering for a large-scale energy storage device, and electrochemical characterization in the area of seawater batteries, which utilize natural seawater as the active material in an open-structured cathode.

**DO-HEE LEE** received the B.S. degree in electrical engineering from the University of Ulsan, in 2007, under the supervision of Prof. Byungwoo Kim. He is currently a Chief Executive Officer (CEO) at STL Company Ltd., an IoT convergence technology solution company. He conducted research on the IoT technology and sensor control using LTE communication.

**YOUNGSIK KIM** received the Ph.D. degree in materials science and engineering from Iowa State University, in 2006, under the supervision of Prof. Steve W. Martin.

After, he joined Prof. John B. Goodenough's Group, The University of Texas at Austin, as a Postdoctoral Fellow. He is currently a Professor with the School of Energy and Chemical Engineering, Ulsan National Institute of Science and Technology (UNIST). He is also the CEO of 4TOONE Corporation, an energy solution company. He conducted research in areas, including lithium- and sodium-ion batteries. Particularly, he is an inventor of the 'sea-water battery,' which is developed as an alternative option for grid-scale energy storage.

**JAE JOON KIM** (Senior Member, IEEE) received the B.S. degree in electronic engineering from Hanyang University, Seoul, South Korea, in 1996, and the M.S. and Ph.D. degrees in electrical engineering from Korea Advanced Institute of Science and Technology, Daejeon, South Korea, in 1998 and 2003, respectively.

From 2000 to 2001, he was with Berkana Wireless, Inc., San Jose, CA, USA (now merged into Qualcomm, Inc.), where he was involved in designing wireless transceivers. From 2003 to 2005, he was with Hynix Semiconductor, Seoul, where he was involved in wireless transceivers and smart-card controllers. From 2005 to 2011, he was the Deputy Director of the Ministry of Information and Communications, Korean Government, and the Ministry of Trade, Industry and Energy. From 2009 to 2011, he was a Research Engineer II with Georgia Institute of Technology, Atlanta, GA, USA. Since 2011, he has been an Associate Professor with Ulsan National Institute of Science and Technology, Ulsan, South Korea. His research interests include integrated circuits for various sensor systems, wireless transceivers, consumer electronics, biomedical appliances, and automotive electronics.